Reinforcement of Optically Healable Supramolecular Polymers with Cellulose Nanocrystals

ARTICLE *in* MACROMOLECULES · DECEMBER 2013

Impact Factor: 5.8 · DOI: 10.1021/ma402143c

8 AUTHORS, INCLUDING:

E. Johan Foster

Virginia Polytechnic Institute and State Univer…

67 PUBLICATIONS **1,056** CITATIONS

Macromolecules

Article

pubs.acs.org/Macromolecules

Reinforcement of Optically Healable Supramolecular Polymers with Cellulose Nanocrystals

Souleymane Coulibaly,[†] Anita Roulin,[†] Sandor Balog,[†] Mahesh V. Biyani,[†] E. Johan Foster,[†] Stuart J. Rowan,[‡] Gina L. Fiore,[†,*] and Christoph Weder[†,*]

[†]Adolphe Merkle Institute, University of Fribourg, CH-1700 Fribourg, Switzerland

[‡]Department of Macromolecular Science and Engineering, Case Western Reserve University, Cleveland, Ohio 44106, United States

Supporting Information

ABSTRACT: We report the preparation and characterization of light-healable nanocomposites based on cellulose nanocrystals (CNCs) and a metallosupramolecular polymer (MSP) assembled from a telechelic poly(ethylene-*co*-butylene) that was end-functionalized with 2,6-bis(1′-methylbenzimidazolyl) pyridine (Mebip) ligands and $Zn(NTf_2)_2$. The polymer absorbs incident ultraviolet (UV) radiation and converts it into heat, which causes dissociation of the metal−ligand motifs. This process liquefies the material, and small defects are readily filled. When the UV light is switched off, the MSP reassembles and the original properties are restored. The introduction of CNCs into the MSP matrix leads to a significant increase of the stiffness and strength, from 52 and 1.7 MPa for the neat polymer to 135 and 5.6 MPa upon introduction of 10% w/w CNCs. The Zn^{2+} ions bind to the CNCs which means the metal:ligand ratio of the MSP must be adjusted accordingly. In nanocomposites thus made, deliberately introduced defects can be efficiently healed.

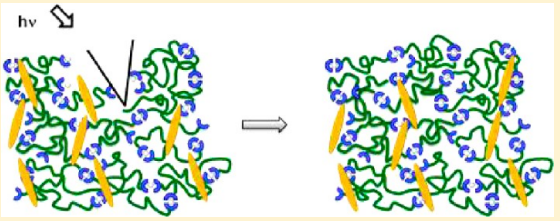

INTRODUCTION

Mechanical malfunctions of polymeric materials are often the result of crack formation and propagation until the material eventually fails.[1] To address this problem and to extend the lifetime and functionality of polymer-based products, researchers have recently developed several approaches to create self-healing or healable polymers, which have the ability to repair themselves autonomously (self-healing materials) or can be healed upon exposure to an external stimulus such as heat, light, pressure, or mechanical stress (healable materials).[1−10] One attractive approach to create such healable materials is the use of supramolecular polymers.[10] These materials are assembled on the basis of noncovalent binding motifs and can, when healing action is desired, be temporarily disassembled upon exposure to an external stimulus. Many of the healable supramolecular polymers studied to date are physically or covalently cross-linked networks with a low glass transition temperature and therefore display moderate strength and stiffness under ambient conditions.

We[11−16] and many others have previously shown that low-modulus polymers can be efficiently reinforced upon introduction of rigid, high-aspect-ratio cellulose nanocrystals (CNCs) isolated by hydrolysis of natural cellulose.[17−20] Recently, Fox et al. used this concept to reinforce supramolecular healable polymers based on $\pi-\pi$ interactions with unmodified CNCs isolated from the mantles of tunicates.[21] This approach was extended to create light-healable nanocomposites based on a telechelic poly(ethylene-*co*-butylene) that was end-capped with hydrogen-bonding ureidopyrimidone groups and CNCs decorated with the same binding motif.[22] Both types of nanocomposites show greatly improved mechanical properties in comparison to the neat supramolecular polymers. A comparison of the two materials systems suggests that dissociation of the reinforcing CNC network during the healing event is important to permit efficient healing. In the former system, this was achieved by limiting the CNC content to 10% w/w.[21,22] While the mechanical properties of damaged nanocomposites with a higher CNC content could be fully restored, the degree of reinforcement was not as good, presumably on account of some phase separation aided by strong CNC−CNC interactions and weaker CNC−matrix interactions. In the hydrogen-bonded nanocomposites, where the CNCs were decorated with the same supramolecular motif used to assemble the supramolecular polymer, deliberately introduced defects could be healed quickly and efficiently, even at a filler content of 20% w/w, i.e., in compositions that exhibit high strength and stiffness.[22] This attractive combination of properties appears to result from the specific design, which leads to full integration of filler and matrix and permits the temporary disengagement of all relevant supramolecular interactions during the healing process.

Here, we report on the preparation and characterization of light-healable nanocomposites based on CNCs and a previously studied metallosupramolecular polymer[23] made by the assembly of $Zn(NTf_2)_2$ and a telechelic poly(ethylene-*co*-butylene) that was end-functionalized with 2,6-bis(1′-methylbenzimidazolyl) pyridine (Mebip) ligands. We have previously reported that the metal−ligand motifs absorb incident

Received: October 17, 2013
Revised: December 10, 2013
Published: December 17, 2013

ultraviolet radiation and serve as light−heat converters.[23] Upon irradiation with UV light, the metal−ligand motifs are temporarily dissociated and the material is transformed into a low-viscosity liquid, which can easily fill small defects. It was shown that when the radiation is switched off, the metallopolymers reassemble and their original properties are restored.[23] Anticipating that the surface hydroxyl groups of the CNCs can bind to the Zn^{2+} ions and thereby connect the reinforcing filler with the matrix,[24,25] we sought to explore how the introduction of this filler affects the mechanical properties and healability of these metallopolymers.

EXPERIMENTAL SECTION

Materials. 2,6-Bis(1′-methylbenzimidazolyl)-4-hydroxypyridine (HOMebip) and zinc bistriflimide ($Zn(NTf_2)_2$) were prepared as previously reported.[23] Microcrystalline cellulose (MCC) was purchased from MFC Biopolymer (NT 100 Latice Avicel). Hydroxyl-terminated poly(ethylene-*co*-butylene) (M_n = 3100 g/mol and PDI = 1.05) was donated by Cray Valley SA (Krasol HLBH-P 3000). To remove acid impurities, $CHCl_3$ was passed through activated basic alumina before use. Tetrahydrofuran was purified by passage through alumina columns.[26] All other solvents and reagents were used as received.

Methods. ^{1}H (300 and 360 MHz) NMR spectra were recorded on a Bruker Advance III spectrometer in $CDCl_3$.^{1}H NMR coupling constants are given in Hz. ^{1}H NMR spectra were referenced against the signal of residual $CHCl_3$ 7.26 ppm. UV−vis spectra were recorded on a Shimadzu UV-2401 PC spectrophotometer in $CHCl_3/CH_3CN$ (9:1). Molecular weights were determined by gel permeation chromatography (GPC) (THF, 40 °C, 1.0 mL/min) using multiangle laser light scattering (MALLS) (λ = 658 nm, 25 °C) and refractive index (λ = 658 nm, 40 °C) detection. A Polymer Laboratories 5 μm mixed-C guard column and two GPC columns along with Wyatt Technology Corp. (Optilab REX interferometric refractometer, miniDawn TREOS laser photometer) and Agilent Technologies instrumentation (series 1200 HPLC) and Wyatt Technology software (ASTRA) were used for the GPC analysis. The incremental refractive index (dn/dc) was estimated by a single-injection method that assumed 100% mass recovery from the columns. Thermogravimetric analyses (TGA) were conducted under N_2 using a Mettler-Toledo STAR thermogravimetric analyzer in the range of 25 to 500 °C with a heating rate of 10 °C/min. Differential scanning calorimetry (DSC) measurements were performed under N_2 using a Mettler-Toledo STAR system modulated differential scanning calorimeter operated in modulated mode (amplitude ±1 °C, period 60 s, heating/cooling rate 10 °C/min, range −70 to 250 °C). Data from the second heating cycle and the reverse heat flow curve are reported unless indicated otherwise (T_d = onset point of decomposition, T_g = glass transition temperature). Dynamic mechanical thermal analyses (DMTA) were conducted under N_2 on a TA Instruments DMA Q 800 with a heating rate of 3 °C/min and a frequency of 1 Hz in the range of −100 to 100 °C, unless indicated otherwise. The stress strain measurements were conducted at 25 °C, with a strain rate of 5%/min. All mechanical tests were conducted on dog-bone-shaped samples. Reported mechanical data are averages of 3−5 independent experiments and all errors are standard deviations. The tensile moduli were calculated from the slopes of the linear region in the strain regime of 0−0.5% strain. The area under the stress−strain curves was determined to quantify the toughness.

Microscopy. Atomic force microscopy (AFM) was carried out on a Nanowizard II (JPK instruments). Images were collected by scanning in tapping mode using a silicon cantilever with a spring constant of 42 N/m at the resonance frequency of 320 kHz. Transmission electron microscopy (TEM) was performed to determine the dimensions of CNCs and the quality of their dispersion in DMF and CH_2Cl_2 on a Phillips Electron Optics CM 100 operated at an accelerating voltage of 80 kV. The dimensions of the CNCs were determined using ImageTool software and by analyzing five randomly selected TEM images of CNC samples deposited from CH_2Cl_2, which resulted in a length L of 200 ± 40 nm, a width D of 20 ± 2.3 nm, and an aspect ratio (L/D) of ∼10.

Cellulose Nanocrystal (CNC) Dispersion. The initial dispersion of MCC in DMF followed the procedure reported by Capadona et al.[27,28] MCC (12.5 g) was added to DMF (1 L) and the mixture was sonicated in a Badelin Sonorex Technik RL 70 UH ultrasound bath for 6 h at 25 °C. The resulting suspension was centrifuged (30 min at 3600 rpm). After the supernatant DMF was decanted, a 9:1 DMF/CH_2Cl_2 solvent mixture (1 L) was added and the dispersion was ultrasonicated for an additional 6 h. Using a procedure reported by Siqueira et al.,[28] the suspension was centrifuged, the supernatant was decanted, and the CNCs were suspended in CH_2Cl_2 (1 L). The dispersion was ultrasonicated for 6 h, and then stirred (1000 rpm) at room temperature for 1 d. The resulting suspension contained a CNC content of 10 ± 1 mg/mL (determined gravimetrically). The CNC suspension was stable for 2 d.

Synthesis of 2,6-Bis(1′methylbenzimidazoyl)-4-oxypyridine-poly(ethylene-*co*-butylene)-2,6-bis(1′-methylbenzimidazolyl)-4-oxypyridine (BKB). The telechelic macromonomer was prepared as previously reported[23] with the following modifications. 2,6-bis(1′-methylbenzimidazolyl)-4-hydroxypyridine (2.07 g, 5.82 mmol), triphenylphosphine (3.05 g, 11.6 mmol), and hydroxyl-terminated poly(ethylene-*co*-butylene) (M_n = 3100 g/mol, 5.41 g, 17.4 mmol) were dried in a vacuum oven at 70 °C for one day. Under a N_2 atmosphere, anhydrous THF (120 mL) was added to the reaction mixture. A solution of diethyl azodicarboxylate (DEAD) (4.25 mL, 40% w/w in toluene, 23.3 mmol) was then added at −40 °C. The reaction mixture was stirred for 4 h at −40 °C and then slowly warmed to room temperature and stirred for an additional 48 h. The reaction mixture was concentrated *in vacuo* and the resulting residue was dissolved in hot hexanes (200 mL). The crude product was washed with CH_3OH (3 × 100 mL) and 1 M aq NaOH (3 × 100 mL). The organic layer was dried over Na_2SO_4, filtered, and then concentrated *in vacuo*. The product was further purified by column chromatography (SiOH, CH_2Cl_2:CH_3OH 100:0, 99:1, 98:2 v/v). The organic fractions were combined and concentrated *in vacuo* to afford the purified product as a tacky white solid (4.9 g, 63% yield). The ^{1}H NMR spectra matched reported values.[23]

UV−Vis Titration of BKB. A solution of BKB (0.22 mg, 25 μM) in a $CHCl_3/CH_3CN$ mixture (9:1 v/v, 2 mL) was titrated with 25 μL aliquots of $Fe(ClO_4)_2$ (526 μM) in the same solvent mixture. The addition was done incrementally and after each aliquot addition of the metal solution the samples were characterized by UV−vis spectroscopy. The absorption at 354 nm was plotted against the concentration of Fe^{2+}. At the point where the slope of this function shows a discontinuity, the Fe^{2+} concentration is assumed to correspond to the BKB concentration; using the assumption that the BKB was fully end-capped, the quantity of $Fe(ClO_4)_2$ solution used at the titration end point, and the amount of BKB in the solution permitted to calculate the number-average molecular weight (M_n) of the BKB (4400 g/mol), which was used to calculate the stoichiometry of the metallopolymers with $Zn(NTf_2)_2$. A titration with $Zn(NTf_2)_2$ was carried out using the same protocol, using the above calculated M_n value and as a result the $Zn(NTf_2)_2$:BKB ratio at the end point was observed.

UV−Vis Titration of BKB in the Presence of CNCs (10% w/w). A solution of BKB (0.44 mg, 49.8 μM) in a 9:1 v/v CH_2Cl_2/CH_3CN mixture (2 mL) was combined with a dispersion of CNCs dispersed in CH_2Cl_2 (104 μL, 10 mg/mL) to create a mixture in which the CNC content represented 10% w/w of the BKB. This mixture was titrated with 25 μL aliquots of $Zn(NTf_2)_2$ (2.04 mg, 326 μM) in a 9:1 v/v CH_2Cl_2:CH_3CN (10 mL) solvent mixture. The addition was done incrementally and after each aliquot addition of the $Zn(NTf_2)_2$ solution the samples were characterized by UV−vis spectroscopy. The normalized absorbance at 354 nm was plotted against the ratio of $Zn(NTf_2)_2$:BKB and the end-point was determined from the discontinuity of the plot.

Synthesis of $[Zn_xBKB](NTf_2)_{2x}$ and Nanocomposites with CNCs. A representative procedure for the preparation of CNC/$[Zn_{0.7}BKB](NTf_2)_{1.4}$ nanocomposite films (10% w/w of CNCs

dx.doi.org/10.1021/ma402143c | *Macromolecules* 2014, 47, 152−160

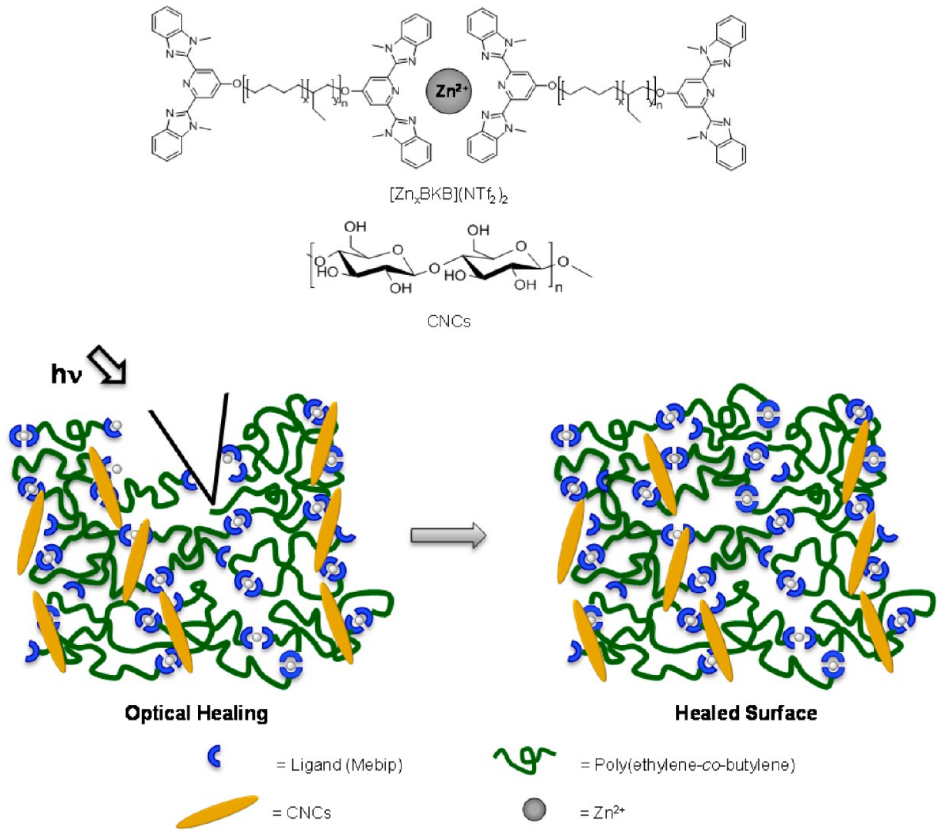

Figure 1. Chemical structure of the metallopolymers $[Zn_xBKB](NTf_2)_{2x}$ and the CNCs and a schematic representation of the metallosupramolecular nanocomposites.

relative to the weight of the BKB) is provided. This procedure serves as an example for the preparation of all nanocomposites films studied and also the CNC-free metallopolymer controls: To a stirred solution of BKB (390 mg, 0.089 mmol) in CH_2Cl_2 (3 mL) a solution of $Zn(NTf_2)_2$ (135 mg, 0.215 mmol,) in anhydrous CH_3CN (1.72 mL) was added. The mixture was stirred for 5 min and a dispersion of CNCs (42 mg, 10 mg/mL suspension) in CH_2Cl_2 (4.2 mL) was added. The mixture was stirred vigorously for 15 min, ultrasonicated for 1 h, and then stirred for an additional 10 min. The solvents were subsequently removed *in vacuo* and the product was further dried overnight.

Fabrication of $[Zn_xBKB](NTf_2)_{2x}$ and CNC/$[Zn_xBKB](NTf_2)_{2x}$ Nanocomposite Films. Films of the neat $[Zn_xBKB](NTf_2)_{2x}$ and of the nanocomposites with CNCs were made by compression molding the materials at a pressure of 3 tons in a Carver press between Teflon sheets at 120 °C for 10 min, using spacers to control the thickness, and subsequently cooled to room temperature to yield 350–400 μm thick films.

Film Damage and Healing. Films of the neat $[Zn_xBKB](NTf_2)_{2x}$ and of the nanocomposites with CNCs were damaged in a controlled manner by cutting the films to a depth of ca. 50–70% of their original thickness. This was done with a custom-built, air-pressure-powered cutting device, in which a razor blade was mounted with its edge parallel to a sample holder and kept at a constant height. The distance between the sample holder and blade could be adjusted with a caliper, thus allowing control over the depth of the cuts that were applied upon drawing the blade across the sample. The damaged samples were then exposed to filtered light from a Honle Bluepoint 4 Ecocure UV source, which emitted light in the range of 320 to 390 nm. The power density was varied between 120 and 950 mW/cm^2 as detailed in the text.

Small-Angle X-ray Scattering (SAXS). The SAXS spectra were recorded with an S-MAX3000 pinhole camera (Rigaku Innovative Technologies, Auburn Hills, MI). The samples were kept in vacuum at room temperature during the measurements. Raw data were processed according to standard procedures, and the scattering spectra are presented as a function of the momentum transfer $q = 4\pi\lambda^{-1}\sin(\theta/2)$, where θ is the scattering angle and λ = 0.1524 nm is the photon wavelength.

RESULTS AND DISCUSSION

Preparation of Metallosupramolecular Nanocomposites. The metallosupramolecular nanocomposites investigated here are based on a previously studied metallosupramolecular polymer[23] resulting from the assembly of $Zn(NTf_2)_2$ and a telechelic poly(ethylene-*co*-butylene) end-functionalized with 2,6-bis(1′-methylbenzimidazolyl) pyridine (Mebip) ligands (Figure 1). The cellulose nanocrystals used in this work were isolated from microcrystalline cellulose (MCC) according to a previously reported protocol, which affords DMF dispersions of the CNCs.[27] Unless their surface is modified with solubilizing groups, CNCs are usually only well dispersible in polar protic solvents such as water and DMSO,[29] which do not permit dissolution of the metallosupramolecular polymer. However, Dufresne and co-workers[28] recently showed that unmodified CNCs from a sisal source can be temporarily suspended in CH_2Cl_2 via a solvent exchange-process. Adaptation of this protocol permitted for the transfer of the CNCs utilized here from DMF into CH_2Cl_2, which proved to be a suitable solvent for the fabrication of the metallosupramolecular nanocomposites (*vide infra*). The resulting CNC suspensions (Figure S1, Supporting Information) were found to be stable for 2 days, before sedimentation of the CNCs was observed. However, it was possible to resuspend the CNCs in CH_2Cl_2 by a combination of stirring and ultrasonication. TEM images of CNCs that were drop-casted from CH_2Cl_2 (Figure 2) confirm

dx.doi.org/10.1021/ma402143c | *Macromolecules* 2014, 47, 152–160

Figure 2. Transmission electron microscopy (TEM) image of CNCs isolated from microcrystalline cellulose (MCC), and deposited from a suspension in CH_2Cl_2 (0.03 mg/mL) onto a TEM grid and dried at 70 °C for 3 h.

that the MCC had indeed been efficiently disintegrated into CNCs and that these CNCs formed homogeneous dispersions in CH_2Cl_2. Analysis of the TEM images revealed that the CNCs transferred into CH_2Cl_2 have an average length of 200 ± 40 nm, a width of 20 ± 2.3 nm, and an aspect ratio of 10. The density of surface charges, presumably stemming from the hydrolysis of the biomass, was determined to be 37 mmol/kg (Figure S2).

To explore possible interactions between the CNCs and the metallosupramolecular polymer, the BKB macromonomer was titrated with $Zn(NTf_2)_2$ in the presence and absence of CNCs and metal−ligand coordination was monitored by UV−vis spectroscopy. The free Mebip ligand features an absorbance band with a maximum, λ_{max}, at 313 nm (Figure 3a). Upon coordination with $Zn(NTf_2)_2$ the absorbance spectrum exhibits a bathochromic shift and the newly formed absorbance of the ligand-to-metal charge transfer (LMCT) transition displays a λ_{max} around 354 nm (Figure S4). Thus, the formation of the metallosupramolecular polymer can be monitored by the decrease of ligand or increase of metal−ligand complex absorbance. Aliquots of $Zn(NTf_2)_2$ were added to a solution of BKB and 10% w/w CNCs (relative to the weight of the BKB) in a 9:1 v/v CH_2Cl_2:CH_3CN solvent mixture; the same experiment was also carried out for the BKB without CNCs. The absorption spectra acquired upon titration of BKB with $Zn(NTf_2)_2$ both in the presence and absence of the CNCs (Figure 3a, Figure S4), exhibit an isosbestic point at 327 nm, reflecting a well-defined equilibrium between the free and metal-coordinated ligand.[23] Figure 3b shows a normalized absorbance at 354 nm as a function of the Zn^{2+}:BKB ratio for both systems (with and without CNCs), indicative of the formation of the MSP of the sum formula $[Zn_xBKB](NTf_2)_{2x}$. In the case of the CNC-free system, the data mirror the previous findings[23] and show a discontinuity of the absorbance change at a Zn^{2+}:BKB ratio of 1:1, corresponding to a Zn^{2+}:Mebip ratio of 1:2. In the presence of 10% w/w CNCs, the saturation point is shifted to a nominal Zn^{2+}:BKB ratio of 1.4:1, indicating that a fraction of the metal ions also bind to the CNCs. This finding is, at least qualitatively, consistent with previous reports that have demonstrated the binding of Zn^{2+} with cellulose,[24,25] and confirms that the CNCs and the metallosupramolecular polymer, as intended, indeed integrate into supramolecular nanocomposites.

Reference films of the neat $[Zn_xBKB](NTf_2)_{2x}$ (Figure 4) were prepared in a similar fashion as recently reported,[23] *i.e.*, by combining BKB and $Zn(NTf_2)_2$ in a mixture of CH_2Cl_2 (instead of previously used $CHCl_3$) and CH_3CN (9:1 v/v), evaporation of the solvent, and subsequent compression-molding. Since it was found that in the case of $[Zn_xBKB](NTf_2)_{2x}$ a Zn^{2+}:BKB ratio of 1:1 results in the best mechanical properties, but limited healability, whereas a Zn^{2+}:BKB ratio of x = 0.7:1 provides for better healability but lower strength and stiffness (the excess of free ligands renders the system more dynamic), both these compositions were used here as reference materials.[23] The possibility to suspend CNCs in CH_2Cl_2 (*vide supra*) provides a means to readily introduce the cellulose nanofiller into these metallosupramolecular polymers, i.e., by combining CNCs, BKB, and $Zn(NTf_2)_2$ in a mixture of CH_2Cl_2 and CH_3CN. Taking into consideration the findings of Fox et al.,[21] who reported that nanocomposites with high CNC content show a reduced reinforcing effect the CNC content was fixed to 10% w/w relative to the BKB. Nanocomposite films with a varying Zn^{2+}:BKB ratio (x) from 0.7−1.5 and a thickness of 350−450 μm were prepared by the same process as used here for films of the neat metallosupramolecular polymers. In view of the observation that in the presence of 10% w/w CNCs about a third of the Zn^{2+} ions bind to the cellulose instead of

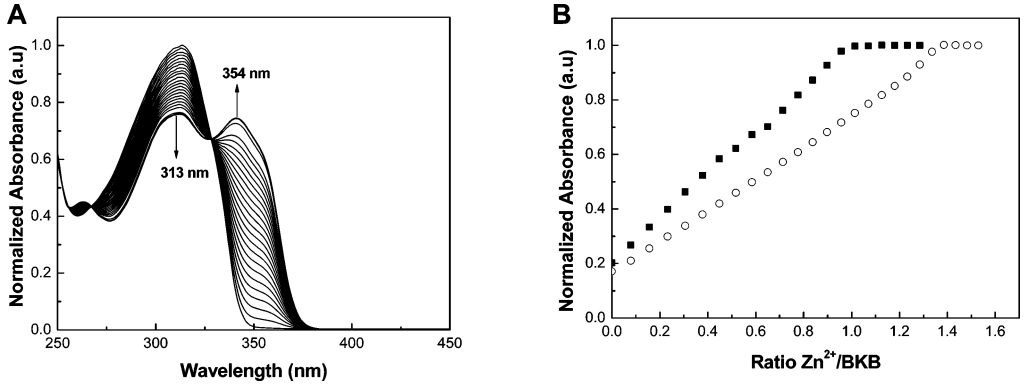

Figure 3. (A) UV−vis spectra acquired upon titration of the macromonomer BKB in the presence of CNCs. Data were acquired upon adding aliquots of $Zn(NTf_2)_2$ to a mixture of BKB (25 μM) and CNCs (2 mg/mL, corresponding to 10% w/w with respect to the BKB) in a CH_2Cl_2/CH_3CN (9:1 v/v) solvent mixture. (B) Absorption at 354 nm of the spectra recorded as a function of the $Zn(NTf_2)_2$:BKB ratio (○). Also shown are the corresponding data for a titration of the neat BKB without CNCs (■) under otherwise identical conditions.

dx.doi.org/10.1021/ma402143c | *Macromolecules* 2014, 47, 152−160

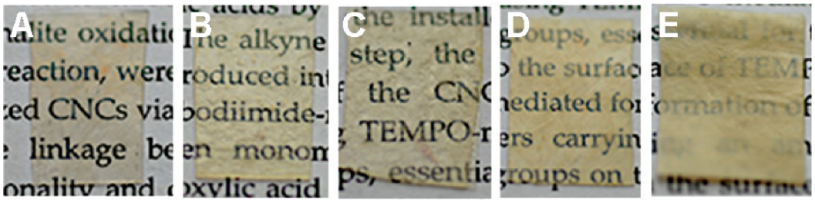

Figure 4. Images of metallosupramolecular nanocomposite films containing 10% w/w CNCs (relative to the BKB) and $[Zn_xBKB](NTf_2)_{2x}$ with varying Zn^{2+}:BKB ratio (x). Key: (A) CNC/$[Zn_{0.7}BKB](NTf_2)_{1.4}$; (B) CNC/$[Zn_{0.8}BKB](NTf_2)_{1.6}$; (C) CNC/$[Zn_{1.0}BKB](NTf_2)_2$; (D) CNC/$[Zn_{1.2}BKB](NTf_2)_{2.4}$; (E) CNC/$[Zn_{1.4}BKB](NTf_2)_{2.8}$.

the BKB (Figure 3b), and that a third of the Mebip ligands should remain free to promote healing, we expected the nanocomposites with $[Zn_{1.0}BKB](NTf_2)_2$ to display the best properties. As can be seen from the pictures in Figure 4, films with a Zn^{2+}:BKB ratio of 0.7−1.0 are transparent, suggesting that the CNCs are well dispersed in the metallosupramolecular polymer. At higher Zn^{2+}:BKB ratios (x = 1.2−1.4) the materials become opaque, suggesting at least partial aggregation of the CNCs, which is likely due to coordination of the excess of Zn^{2+} to the CNCs. Attempts to create nanocomposites with higher CNC content were made, but they did not show the expected mechanical properties (*vide infra*).

Morphological Characterization. Small-angle X-ray scattering (SAXS) experiments were performed to determine the influence of the CNCs on the morphology of the metallosupramolecular materials. We note that SAXS and transmission electron microscopy (TEM) studies of films of $[Zn_xBKB](NTf_2)_{2x}$ revealed microphase-segregated lamellar morphologies in which the metal−ligand complexes form a hard phase that physically cross-links the soft domains formed by the poly(ethylene-*co*-butylene) segment.[23,30] The SAXS data (Figure 5) of the CNC/$[Zn_xBKB](NTf_2)_{2x}$ nanocomposites

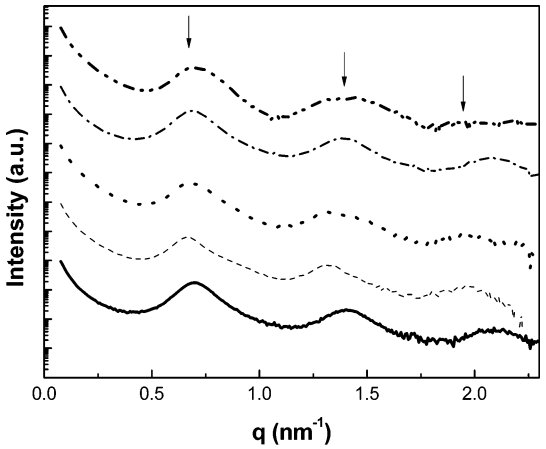

Figure 5. SAXS data for CNC/$[Zn_xBKB](NTf_2)_{2x}$ nanocomposites containing 10% w/w CNCs (relative to the BKB) with varying Zn^{2+}:BKB ratio x: (——) CNC/$[Zn_{0.7}BKB](NTf_2)_{1.4}$; (---) CNC/$[Zn_{0.8}BKB](NTf_2)_{1.6}$; (···) CNC/$[Zn_{1.0}BKB](NTf_2)_2$; (—·—) CNC/$[Zn_{1.2}BKB](NTf_2)_{2.4}$; (——··——) CNC/$[Zn_{1.4}BKB](NTf_2)_{2.8}$.

with varying Zn^{2+}:BKB ratio show distinct correlated Bragg diffraction peaks up to the third order, which confirm that also the nanocomposites with CNC adopt well-ordered lamellar morphologies. The long period is *ca.* 10 nm, and was determined to be independent of the Zn^{2+}:BKB ratio (x) in these materials. This spatial distance is similar to that observed for the neat $[Zn_xBKB](NTf_2)_{2x}$, for which a spatial distance of *ca.* 8.5 nm was observed.[23] We note that the scattering patterns were isotropic, indicating that the domains are not oriented. Interestingly, the lamellar morphology is not perturbed by the presence of CNCs, which have dimensions (diameter = 20 ± 2.3 nm, length = 200 ± 40 nm) that are much larger than the long period of the lamellar morphology.

Mechanical Properties. The mechanical properties of thin films of the CNC/$[Zn_xBKB](NTf_2)_{2x}$ nanocomposites were explored as a function of temperature by dynamic mechanical thermal analysis (DMTA) (Figure 6, Table 1, Figure S6, Table

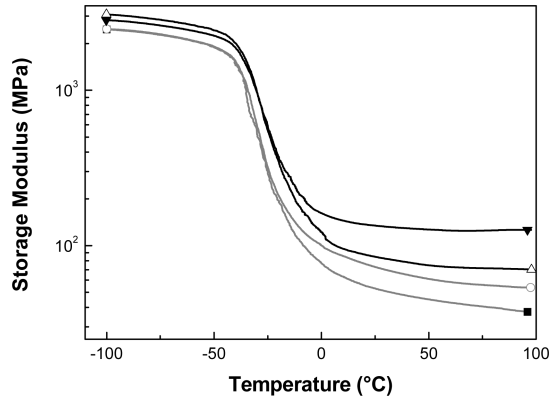

Figure 6. Representative dynamic mechanical thermal analysis (DMTA) traces of the neat metallopolymers $[Zn_{0.7}BKB](NTf_2)_{1.4}$ (■) and $[Zn_{1.0}BKB](NTf_2)_2$ (○) and of the nanocomposites containing 10% w/w CNC and $[Zn_{1.0}BKB](NTf_2)_2$ (△) or $[Zn_{1.4}BKB](NTf_2)_{2.8}$ (▼). The experiments were conducted at a heating rate of 3 °C/min and a frequency of 1 Hz under N_2. Other compositions were also explored; data are shown in Figures S6 and S14a and Table 1, and Table S1.

S1) and at room temperature by means of tensile testing (Figure 7, Table 1, Figure S5). The mechanical properties of neat films of $[Zn_{0.7}BKB](NTf_2)_{1.4}$ and $[Zn_{1.0}BKB](NTf_2)_2$ were also determined for the purpose of comparison; similar results to previously reported data were obtained for these materials.[23] The DMTA traces of the neat metallosupramolecular polymers, $[Zn_{0.7}BKB](NTf_2)_{1.4}$ and $[Zn_{1.0}BKB](NTf_2)_2$, display a glassy regime below −23 °C, where the tensile storage modulus E' is ∼2 GPa (Figure 6). Above the glass transition a broad rubbery plateau is observed and at 25 °C $[Zn_{0.7}BKB](NTf_2)_{1.4}$ and $[Zn_{1.0}BKB](NTf_2)_2$ display storage moduli of 52 and 60 MPa, respectively. Thus, as previously reported, the stiffness of these materials decreases as the Zn^{2+}:BKB ratio is offset. Stress−strain experiments conducted at 25 °C reveal Young's moduli that mirror this trend and result a maximum stress at break of 1.7 MPa for $[Zn_{0.7}BKB](NTf_2)_{1.4}$ and 4.7 MPa for $[Zn_{1.0}BKB](NTf_2)_2$ (Figure 7, Table 1).

dx.doi.org/10.1021/ma402143c | *Macromolecules* 2014, 47, 152−160

Table 1. Mechanical Properties of $[Zn_xBKB](NTf_2)_{2x}$ and CNC/$[Zn_xBKB](NTf_2)_{2x}$ Nanocomposites

sample	storage modulus[a] (MPa)	Young's modulus[b] (MPa)	maximum stress[b] (MPa)	strain at break[b] (%)	toughness[b] (10^7 J/m^3)
			$[Zn_{0.7}BKB](NTf_2)_{1.4}$		
original	52 ± 1.0	31 ± 2.2	1.7 ± 0.4	23 ± 5	2.3 ± 0.2
damaged[c]			0.7 ± 0.1	8 ± 1	0.3 ± 0.1
healed[d]		39 ± 5.4	1.5 ± 0.2	30 ± 2	2.9 ± 0.3
			$[Zn_{1.0}BKB](NTf_2)_2$		
original	60 ± 1.4	61 ± 0.7	4.7 ± 0.3	21 ± 1	6.5 ± 0.4
damaged[c]			3.7 ± 0.2	14 ± 1	3.5 ± 1.1
healed[d]		41 ± 1.8	4.0 ± 0.1	15 ± 3	4.1 ± 0.7
			CNC/$[Zn_{0.7}BKB](NTf_2)_{1.4}$		
original	77 ± 1.1	35 ± 1.6	3.3 ± 0.2	17 ± 2	2.5 ± 0.1
damaged[c]			0.5 ± 0.1	8 ± 2	0.2 ± 0.1
healed[d]		32 ± 2.1	2.8 ± 0.5	14 ± 1	2.3 ± 0.3
			CNC/$[Zn_{0.8}BKB](NTf_2)_{1.6}$		
original	85 ± 1.4	60 ± 0.5	4.8 ± 0.2	26 ± 2	8.7 ± 0.3
damaged[c]			1.3 ± 0.1	6 ± 2	1.3 ± 1.0
healed[d]		40 ± 6.2	3.4 ± 0.5	23 ± 4	5.7 ± 0.1
			CNC/$[Zn_{1.0}BKB](NTf_2)_2$		
original	86 ± 6.0	62 ± 10	4.7 ± 0.7	26 ± 1	7.9 ± 0.2
damaged[c]			1.3 ± 0.2	7 ± 3	1.2 ± 1.2
healed[d]		61 ± 8.0	4.6 ± 0.6	24 ± 2	7.7 ± 0.5
			CNC/$[Zn_{1.2}BKB](NTf_2)_{2.4}$		
original	101 ± 2.0	99 ± 1.3	4.8 ± 1.6	12 ± 3	4.0 ± 0.3
damaged[c]			3.5 ± 0.1	12 ± 1	2.6 ± 0.3
healed[d]		93 ± 4.5	4.8 ± 1.6	14 ± 3	3.3 ± 1.0
			CNC/$[Zn_{1.4}BKB](NTf_2)_{2.8}$		
original	135 ± 3.0	101 ± 1.9	5.6 ± 0.2	12 ± 1	4.7 ± 0.2
damaged[c]			3.6 ± 0.1	12 ± 1	3.0 ± 0.2
healed[d]		97 ± 1.4	5.1 ± 0.7	12 ± 3	3.5 ± 0.6
			CNC/$[Zn_{1.5}BKB](NTf_2)_3$		
original	50 ± 3.0	36 ± 3.0	1.0 ± 0.2	9 ± 2	2.7 ± 0.4

[a]Measured by DMTA at 25 °C. [b]Measured by stress−strain experiments at 25 °C. [c]Samples were damaged in a controlled manner by cutting them to a depth of ∼50−70% of their original thickness. [d]Samples were optically healed by exposure to light of a wavelength of 320 to 390 nm and a power density of 950 mW/cm^2 in case of the neat metallopolymers, 350 mW/cm^2 in case of nanocomposites with a Zn^{2+}:BKB ratio x = 0.7−1, and 120 mW/cm^2 in the case of nanocomposites with a Zn^{2+}:BKB ratio x = 1.2−1.4. Data represent averages from three independently made compositions, from which at least three samples per film were measured.

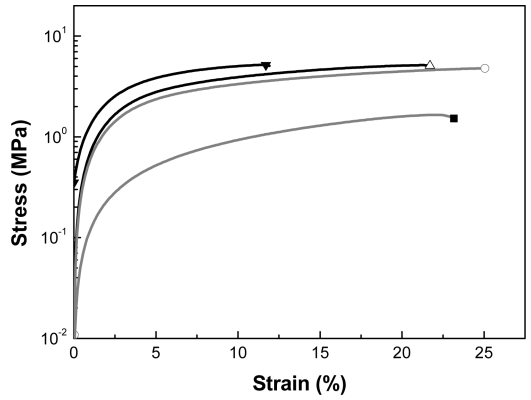

Figure 7. Representative stress−strain curves of the neat metallopolymers $[Zn_{0.7}BKB](NTf_2)_{1.4}$ (■) and $[Zn_{1.0}BKB](NTf_2)_2$ (○) and of CNC/$[Zn_{1.0}BKB](NTf_2)_2$ (△) or CNC/$[Zn_{1.4}BKB](NTf_2)_{2.8}$ (▼) nanocomposites containing 10% w/w of CNCs. The experiments were conducted at 25 °C. Other compositions were also explored; data are shown in Figure S5.

Gratifyingly, the incorporation of CNCs into the $[Zn_xBKB](NTf_2)_{2x}$ matrix led to the desired reinforcement of the metallosupramolecular polymers. Analysis of CNC/$[Zn_xBKB](NTf_2)_{2x}$ nanocomposites by DMTA reveals that the materials possess a tensile storage modulus (E') of 2.8−3.1 GPa at −100 °C, which is about 50% higher than in case of the neat $[Zn_xBKB](NTf_2)_{2x}$ (Figure 6, Table 1, Figure S6, Table S1). Also in this series, E' is drastically reduced at temperatures above the glass transition. However, the rubbery plateau is shifted to higher moduli in comparison to the two neat reference metallopolymers studied. The E' at 25 °C increased steadily with increasing Zn^{2+}:BKB ratio from 77 MPa for CNC/$[Zn_{0.7}BKB](NTf_2)_{1.4}$ to 135 MPa for CNC/$[Zn_{1.4}BKB](NTf_2)_{2.8}$ (Figure S6). Thus, in comparison to the stiffest matrix polymers ($[Zn_{1.0}BKB](NTf_2)_2$), E'=60 MPa) the room-temperature modulus of the CNC/$[Zn_xBKB](NTf_2)_{2x}$ nanocomposites is increased by a factor of up to 2.5. An inspection of the DMTA traces further shows that the CNCs stabilize the rubbery plateau, *i.e.*, below 100 °C, E' remains relatively constant as a result of stabilization of the CNC network, whereas a steady decrease is observed at increasing temperature in the case of the neat metallopolymers. It should be noted that at higher Zn^{2+} content (greater than the end point of titration with CNCs), a decrease of E' at 25 °C (50 MPa) was observed for a composition of CNC/$[Zn_{1.5}BKB](NTf_2)_3$ (Figure S14a, Table 1). This behavior is likely due to limitations of the degree of polymerization of the MSP, on account of the excess Zn^{2+}. Therefore, a balance between CNC content and Zn^{2+}

dx.doi.org/10.1021/ma402143c | Macromolecules 2014, 47, 152−160

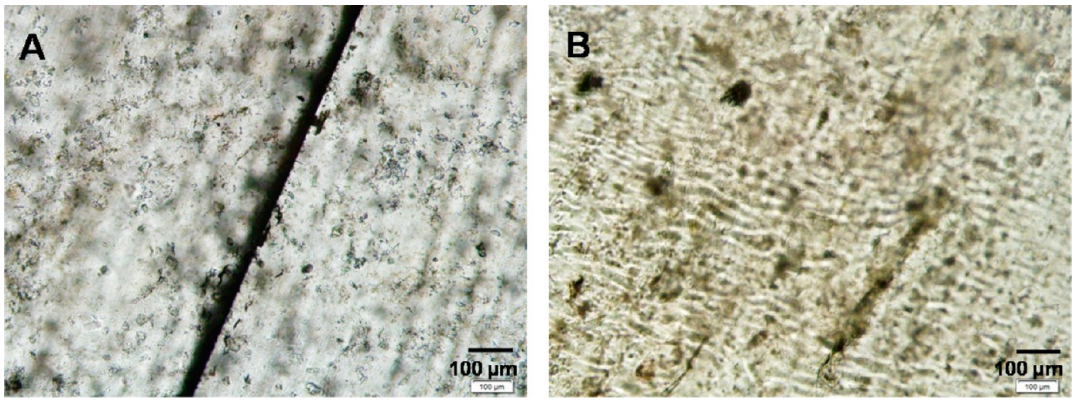

Figure 8. Optical microscopy images of a deliberately damaged CNC/$[Zn_{0.7}BKB](NTf_2)_{1.4}$ nanocomposite film containing 10% w/w CNCs (A) before and (B) after healing through exposure to UV light (320−390 nm, 30 s, 350 mW/cm^2).

concentration is necessary to obtain nanocomposite films with improved mechanical properties. Attempts to create nanocomposites with a CNC content of 15 and 20% w/w were made, but the resulting materials Young's moduli and maximum stresses were lower than those of the materials with only 10% w/w CNCs (Figure S15, Table S2). This behavior mirrors the observations made by Fox et al. for nanocomposites based on a supramolecular polymer assembled through $\pi-\pi$ interactions with unmodified CNCs,[21] and is consistent with aggregation of the filler.

The DMTA results were complemented with tensile tests (Figure 7, Table 1, Figure S5). The Young's modulus changed in a similar manner to E' (Figure 7, Table 1, Figure S5), the maximum stress increased from 1.7 MPa ($[Zn_{0.7}BKB](NTf_2)_{1.4}$) to 3.3 MPa (CNC/$[Zn_{0.7}BKB](NTf_2)_{1.4}$) to 5.6 MPa (CNC/$[Zn_{1.4}BKB](NTf_2)_{2.8}$), further confirming the reinforcement of $[Zn_xBKB](NTf_2)_{2x}$ with CNCs and highlighting the importance of the Zn^{2+}:BKB ratio.

Optical Healing. To explore the healing behavior of CNC/$[Zn_xBKB](NTf_2)_{2x}$ nanocomposites, films of a thickness of 350−400 μm were intentionally damaged by introducing a well-defined cut across the entire sample, with a depth that corresponds to 50−70% of the sample thickness (Figure 8a,11a, and Figures S7 and S9). The samples were subsequently irradiated with UV light of a wavelength range of 320−390 nm, i.e., in the regime where the metal−ligand complexes display a strong absorption band (Figure 3a). In the case of the previously studied neat metallopolymers $[Zn_{0.7}BKB](NTf_2)_{1.4}$ and $[Zn_{1.0}BKB](NTf_2)_2$, which were measured for reference purposes, the incident intensity was set to 950 mW/cm^2, corresponding to the conditions employed in the previous study. In the case of the new nanocomposites, the intensity was reduced to 350 mW/cm^2 for nanocomposites with a Zn^{2+}:BKB ratio of 0.7−1, and to 120 mW/cm^2 in the case of nanocomposites with a Zn^{2+}:BKB ratio of 1.2−1.4, as the samples were found to heat excessively at higher intensities; even at the lower intensities used, a rapid temperature increase to >220 °C was observed (Figure S10). Visual inspection confirmed that in all of the materials (Figures 8, 11, and Figures S7, S9, and S11), except for the neat metallopolymer $[Zn_{1.0}BKB](NTf_2)_2$, and the CNC/$[Zn_{1.5}BKB](NTf_2)_3$ nanocomposite, the damage imparted to the films could completely or largely be removed by this treatment. Atomic force microscopy images (Figure 11) of a CNC/$[Zn_{0.7}BKB](NTf_2)_{1.4}$ nanocomposite film containing 10% w/w CNCs film show that

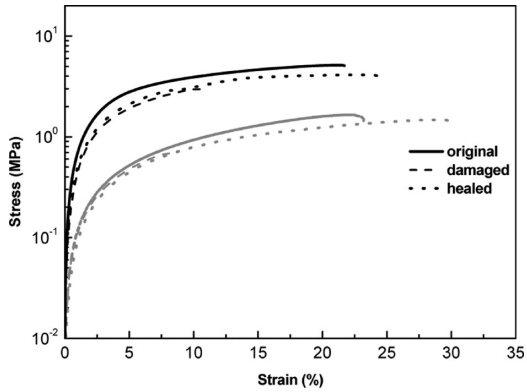

Figure 9. Representative stress−strain curves of films of the neat metallopolymer $[Zn_{0.7}BKB](NTf_2)_{1.4}$ (gray) and of the CNC/$[Zn_{1.0}BKB](NTf_2)_2$ nanocomposites comprising 10% w/w CNC (black). Shown are data acquired at 25 °C for original (——), damaged (- - -), and healed (···) samples. Samples were damaged by applying a cut of a depth of 50−70% of the thickness and healed through a 30 s exposure to light of a wavelength of 320−390 nm and an intensity of 950 mW cm^{-2} in case of the neat metallopolymer and 350 mW cm^{-2} in case of the nanocomposite.

the damage zone is indeed filled and the defect completely disappears.

To quantify the healing efficiency of the nanocomposites films, samples of the various compositions were damaged and healed as described above and the mechanical properties of "original", "damaged", and "healed" samples were explored by tensile testing (Table 1, Figure 9, and Figure S5). The healing efficiency was determined by dividing the average toughness of "original" and "healed" samples. In Figure 9, representative stress−strain curves of films of the neat metallosupramolecular polymer $[Zn_xBKB](NTf_2)_{2x}$ and the nanocomposite CNC/$[Zn_{1.0}BKB](NTf_2)_2$ are shown (the corresponding data for all other compositions are shown in Figure S5 and Table 1). The data show that in all compositions, the stress and strain at break of damaged samples are significantly reduced in comparison to the original materials. Conversely, the original mechanical properties of the materials are largely restored upon UV irradiation (Table 1, Figure 10). A comparison of the data shows that the toughness of healed samples is either statistically indifferent or only slightly lower than the toughness of the original nanocomposites, *i.e.*, the original mechanical properties are nearly fully recovered. While the detailed morphology of the healed zones is yet to be investigated, the mechanical properties

dx.doi.org/10.1021/ma402143c | *Macromolecules* 2014, 47, 152−160

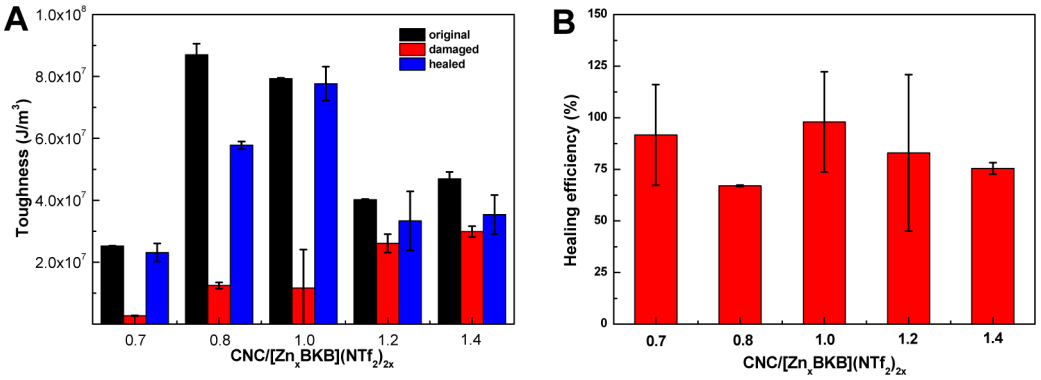

Figure 10. (A) Toughness of original, damaged, and healed CNC/$[Zn_xBKB](NTf_2)_{2x}$ nanocomposite films containing 10% w/w CNCs. The toughness was calculated from the area under the stress−strain curves and represents an average for n = 3−5 measurements; error bars express standard deviation. (B) Healing efficiency of the metallosupramolecular nanocomposite films (n = 3−5 ± standard deviation). Samples were damaged in a controlled manner by cutting them to a depth of ∼50−70% of their original thickness and optically healed by exposure to light of a wavelength of 320 to 390 nm and a power density of 950 mW/cm^2 in case of the neat metallopolymers, 350 mW/cm^2 in case of nanocomposites with a Zn^{2+}:BKB ratio x = 0.7−1, and 120 mW/cm^2 in the case of nanocomposites with a Zn^{2+}:BKB ratio x = 1.2−1.4.

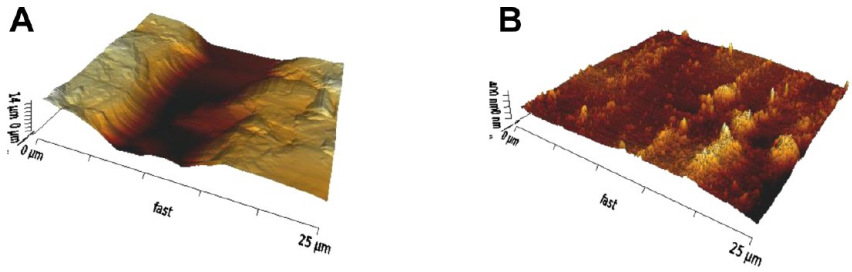

Figure 11. AFM images of a damaged CNC/$[Zn_{0.7}BKB](NTf_2)_{1.4}$ nanocomposite film containing 10% w/w CNCs (A) before and (B) after healing with UV light (320−390 nm, 30 s, 350 mW/cm^2).

suggest that both the metallopolymer and the CNCs flow back into the previously damaged area and that the original nanocomposite is largely restored. These results are in agreement with recently published work from our group based on supramolecular nanocomposites composed of a hydrogen-bonded supramolecular polymer and cellulose nanocrystals.[22]

CONCLUSIONS

In conclusion, this work demonstrates that metallosupramolecular polymers can be reinforced with cellulose nanocrystals to afford nanocomposites with increased stiffness and strength. Our investigation has shown that the CNCs bind with the Zn^{2+} ions used to assemble the MSP, which integrates them into the metallopolymer without changing its morphology. In a certain parameter space, these nanocomposites are optically healable and represent a significant higher strength and stiffness than the neat metallopolymer. Healability is achieved through the circumstance that polymer absorbs incident ultraviolet light and converts it into heat, which causes dissociation of the metal−ligand motifs and presumably also metal-CNC complexes. This process liquefies the material, and small defects are readily filled. Upon removal of UV irradiation, the metallopolymer reassembles and solidifies, thus allowing for efficient healing of these materials. While the detailed morphology of the healed zones is yet to be investigated, the mechanical properties suggest that both the metallopolymer and the CNCs flow back into the healed zone and that the original nanocomposite is restored. A comparison of the mechanical data of original and healed nanocomposites reveals that the amount of Zn^{2+} ions used is very important, as it influences both healability and maximum strength/stiffness. At low Zn^{2+} content, the metallopolymer is of low molecular weight, whereas at high Zn^{2+} content the materials become opaque, suggesting at least partial aggregation of the CNCs due to coordination of the excess of Zn^{2+} to the CNCs. As a consequence of the tunable nature of the polymer backbone, ligands, and metal ions, the general design framework presented here lends itself to be used in connection with other polymer building blocks and architectures, binding motifs, and stimuli.

ASSOCIATED CONTENT

Supporting Information

Images of dispersed CNCs, conductometric titration data, UV−vis spectra, representative stress−strain curves, dynamic mechanical thermal analysis traces, storage moduli data, AFM images, images of nanocomposite films, optical microscopy images, surface temperature plots, images of a dog-bone-shaped sample of CNC/$[Zn_{0.7}BKB](NTf_2)_{1.4}$, thermogravimetric analysis traces, dynamic scanning calorimetry traces, and mechanical properties of nanocomposite films. This material is available free of charge via the Internet at http://pubs.acs.org.

AUTHOR INFORMATION

Corresponding Authors

*E-mail: (G.L.F.) gina.fiore@unifr.ch.
*E-mail: (C.W.) christoph.weder@unifr.ch.

Notes

The authors declare no competing financial interest.

■ ACKNOWLEDGMENTS

We acknowledge funding from the Swiss National Science Foundation (200021_13540/1 and R'Equip 206021_128728), the US Army Research Office (W911NF-09-1-0288 and W911NF-06-1-0414) and the Adolphe Merkle Foundation. We thank Dr. P. Annamalai for fruitful discussions and assistance with the conductometric titration and dispersions of CNCs experiments. We also thank S. Camarero-Espinosa for AFM experiments.

■ REFERENCES

(1) Bergman, S. D.; Wudl, F. *J. Mater. Chem.* **2008**, *18*, 41−62.
(2) Burattini, S.; Greenland, B. W.; Chappell, D.; Colquhoun, H. M.; Hayes, W. *Chem. Soc. Rev.* **2010**, *39*, 1973−1985.
(3) Murphy, E. B.; Wudl, F. *Prog. Polym. Sci.* **2010**, *35*, 223−251.
(4) Urban, M. W. *Prog. Polym. Sci.* **2009**, *34*, 679−687.
(5) Blaiszik, B. J.; Kramer, S. L. B.; Olugebefola, S. C.; Moore, J. S.; Sottos, N. R.; White, S. R. *Ann. Rev. Mater. Res.* **2010**, *40*, 179−211.
(6) Wool, R. P. *Soft Matter* **2008**, *4*, 400−418.
(7) Seiffert, S.; Sprakel, J. *Chem. Soc. Rev.* **2012**, *41*, 909−930.
(8) Wu, D. Y.; Meure, S.; Solomon, D. *Prog. Polym. Sci.* **2008**, *33*, 479−522.
(9) Syrett, J. A.; Becer, C. R.; Haddleton, D. M. *Polym. Chem.* **2010**, *1*, 978−987.
(10) Fiore, G. L.; Rowan, S. J.; Weder, C. *Chem. Soc. Rev.* **2013**, *42*, 7278−7288.
(11) Camarero Espinosa, S.; Kuhnt, T.; Foster, E. J.; Weder, C. *Biomacromolecules* **2013**, *14*, 1223−1230.
(12) Changsarn, S.; Mendez, J. D.; Shanmuganathan, K.; Foster, E. J.; Weder, C.; Supaphol, P. *Macromol. Rapid Commun.* **2011**, *32*, 1367−1372.
(13) Dagnon, K. L.; Shanmuganathan, K.; Weder, C.; Rowan, S. J. *Macromolecules* **2012**, *45*, 4707−4715.
(14) Kumar, S.; Hofmann, M.; Steinmann, B.; Foster, E. J.; Weder, C. *ACS Appl. Mater. Interfaces* **2012**, *4*, 5399−5407.
(15) Mendez, J.; Annamalai, P. K.; Eichhorn, S. J.; Rusli, R.; Rowan, S. J.; Foster, E. J.; Weder, C. *Macromolecules* **2011**, *44*, 6827−6835.
(16) Way, A. E.; Hsu, L.; Shanmuganathan, K.; Weder, C.; Rowan, S. J. *ACS Macro Lett.* **2012**, *1*, 1001−1006.
(17) Eichhorn, S. J.; Dufresne, A.; Aranguren, M.; Marcovich, N. E.; Capadona, J. R.; Rowan, S. J.; Weder, C.; Thielemans, W.; Roman, M.; Renneckar, S.; Gindl, W.; Veigel, S.; Keckes, J.; Yano, H.; Abe, K.; Nogi, M.; Nakagaito, A. N.; Mangalam, A.; Simonsen, J.; Benight, A. S.; Bismarck, A.; Berglund, L. A.; Peijs, T. *J. Mater. Sci.* **2010**, *45*, 1−33.
(18) Habibi, Y.; Lucia, L. A.; Rojas, O. J. *Chem. Rev.* **2010**, *110*, 3479−3500.
(19) Klemm, D.; Kramer, F.; Moritz, S.; Lindström, T.; Ankerfors, M.; Gray, D.; Dorris, A. *Angew. Chem., Int. Ed.* **2011**, *50*, 5438−5466.
(20) Eichhorn, S. J. *ACS Macro Lett.* **2012**, *1*, 1237−1239.
(21) Fox, J.; Wie, J. J.; Greenland, B. W.; Burattini, S.; Hayes, W.; Colquhoun, H. M.; Mackay, M. E.; Rowan, S. J. *J. Am. Chem. Soc.* **2012**, *134*, 5362−5368.
(22) Biyani, M. V.; Foster, E. J.; Weder, C. *ACS Macro Lett.* **2013**, *2*, 236−240.
(23) Burnworth, M.; Tang, L.; Kumpfer, J. R.; Duncan, A. J.; Beyer, F. L.; Fiore, G. L.; Rowan, S. J.; Weder, C. *Nature* **2011**, *472*, 334−337.
(24) Richards, N. J.; Williams, D. G. *Carbohydr. Res.* **1970**, *12*, 409−420.
(25) Xu, Q.; Chen, L.-F. *J. App. Polym. Sci.* **1999**, *71*, 1441−1446.
(26) Pangborn, A. B.; Giardello, M. A.; Grubbs, R. H.; Rosen, R. K.; Timmers, F. J. *Organometallics* **1996**, *15*, 1518−1520.
(27) Capadona, J. R.; Shanmuganathan, K.; Trittschuh, S.; Seidel, S.; Rowan, S. J.; Weder, C. *Biomacromolecules* **2009**, *10*, 712−716.
(28) Siqueira, G.; Bras, J.; Dufresne, A. *Biomacromolecules* **2009**, *10*, 425−432.
(29) van den Berg, O.; Capadona, J. R.; Weder, C. *Biomacromolecules* **2007**, *8*, 1353−1357.
(30) Kumpfer, J. R.; Wie, J. J.; Swanson, J. P.; Beyer, F. L.; Mackay, M. E.; Rowan, S. J. *Macromolecules* **2011**, *45*, 473−480.